Solar Panel Power Generator with Automatic Charging using PWM System Based on Microcontroller

Sulistyo Widodo[1,*], Erfiana Wahyuningsih[2], and Yohanes Galih Adhiyoga[3]

[1,2,3]Universitas Dian Nusantara, 11470, Indonesia

*Corresponding email: sulistyo.widodo@undira.ac.id

Abstract: The growing interest in solar energy as a sustainable and renewable power source has led to a focus on solar power generation systems, including standalone photovoltaic systems, on-grid systems, and hybrid organic/inorganic semiconductor pn-junctions. The literature review of existing research results suggests that the solution to the problem lies in the design and implementation of efficient solar power generation systems. This includes hardware design with specific components such as solar panels, voltage sensors, current sensors, push buttons, and microcontrollers. The research results show that systems can automatically charge energy using sunlight and turn the lights to 7 W. Using the charging system automatically uses pulse width modulation to reduce the risk of damage to the battery because, in the charging process, battery conditions will be monitored. The maximum power generated from solar panel modules used is 35.57 W.

Keywords: battery, charge, pulse width modulation, solar panel

1 Introduction

In 1.5 days, the sun provides 1.7×1022 J of energy. The magnitude of this energy is equivalent to the cumulative energy output attainable from the entirety of Earth's oil reserves, estimated at 3 trillion barrels. Humans consume 4.6×10^{20} J of energy annually. The sun provides this amount of energy in one hour. The sun's energy can more than suffice to power the entire world [1].

The amount of solar radiation harnessed generally determines how much electrical energy a solar power system produces. Consequently, technology for the collection of solar

energy has seen widespread adoption in Indonesia. Solar energy harvesting can be implemented both on and off the grid [2, 3].

Indonesia was previously a significant oil and gas producer, but crude oil production has declined since 1995 (1.6 million barrels per day), while natural gas production has plateaued recently (BP 2015). Consequently, there has been a growing dependence on expensive crude oil and petroleum derivatives imports. Indeed, since 2004, the country has imported oil [4].

In December 2016, PT. PLN (Indonesian government-owned electricity company) raised electricity prices from category R-1 to B-2, becoming Rp 1.472.72/kWh. With the release of the ministerial regulations, ESDM RI No. 3 2014 then applied "Tarif Adjustment" so that the basic electricity fare would follow world oil prices, exchange rate, and inflation rate every month [5]. Therefore, there is a need to utilize alternative energy that is not dependent on oil or gas. One alternative energy is using solar light energy. Indonesia, near the equator, has a mean sun radiation of 4.8 kWh/m2/day, making it ideal for renewable energy [6].

In a study authored by Baimel *et al.* [7] in 2019, two novel maximum power point tracking (MPPT) techniques for photovoltaic (PV) systems were proposed and validated. These approaches aim to enhance the conventional fractional open circuit voltage (FOCV) method. This study evaluates the effectiveness of various MPPT methods, such as Semi-Pilot Cell and Semi-Pilot Panel, in accurately estimating the maximum power point voltage. The SPP-FOCV method is found to be effective in estimating Vmpp at different irradiance levels while keeping the cell temperature constant. Additionally, the SPP-FOCV method provides reliable estimates even under partial shading conditions. The study also shows that the new MPPT methods improve the performance of PV systems compared to the conventional FOCV method.

The current study by Liqun Shang, 2020, aims to assess the efficacy of the Perturb and Observe (P and O) algorithm for MPPT when employed with a buck-boost charge controller in solar systems, building upon prior research conducted by Liqun Shang in 2020.The Proposed incremental conductance approach for MPPT yields greater stability and accuracy compared to standard algorithms. Enhanced tracking speed by 20% to 30% across various ranges of irradiance variation, Resolved the problem of misjudgment during changes in irradiance. The suggested algorithm resulted in a decrease in response time from 0.39 seconds to 0.30 seconds, compared to the old algorithm. Similarly, the response time improved from 0.43 seconds to 0.35 seconds with the proposed algorithm. Additionally, the average output powers of the PV array were somewhat higher when using the proposed algorithm [8].

In 2021, Bhan *et al.* [9] published an article that introduces an improved incremental conductance approach for MPPT in PV systems. This technique builds upon the findings of previous research. The charge controller employs the Perturb and Observe (PO) algorithm to optimize the charging current and efficiently regulate the battery voltage until it approaches maximum capacity. The voltage is monitored using a voltage sensor, which adjusts the duty cycle to operate at the maximum power point (MPP) and maintain the photovoltaic voltage. The investigation resulted in an enhancement of system performance in various weather and loading conditions through the implementation of a buck-boost charge controller.

The literature review offers insights into designing and implementing efficient solar power generation systems, including hardware components like solar panels, voltage sensors, current sensors, push buttons, and microcontrollers. The use of inverter systems with

sinusoidal wave generators and power amplifier driver components is crucial for efficient solar power generation.

This research aims to develop a solar panel power generator system using a microcontroller and pulse width modulation (PWM) to control the charging process automatically by setting the duty cycle depending on battery condition. The novelty of the solution offers a comprehensive testing and evaluation of the solar panel system's operational performance and efficiency under various load conditions, providing significant insights into its performance and efficiency. The goal of this research is to develop a system that is capable of converting solar energy into electrical energy on its own and storing the electrical energy in a battery so that it can be used as an alternative source of energy and help reduce electricity consumption from PT. PLN.

2   Research Method

This section discusses hardware design, block input, block proses, and block output.

2.1   Hardware Design

This paper outlines a methodical approach to the design, implementation, and testing of a solar panel power generation system that incorporates automated charging. The system comprises four primary components: power, input, process, and output. The power block consists of a 12 V battery and a DC-DC Converter 5 V, whilst the input block comprises a solar panel, voltage sensors, current sensors, and push buttons. The process block comprises a 15 V DC-DC Converter, a 2-controller driver circuit, and an ATmega328P microprocessor. The output block consists of an LCD (Liquid Crystal Display) and an Inverter DC–AC (Direct Current to Alternating Current). To evaluate the power generation capabilities of the solar panels, the open-circuit voltage and short-circuit current are measured in direct sunlight. The system's efficiency is assessed during periods of high demand, and data is gathered from both the solar panels and the inverter. This extensive testing methodology offers valuable insights into the system's performance and efficiency when subjected to real-world situations.

MPPT is a method employed in PV systems to optimize power generation by operating panels at their highest efficiency point. The MPPT approach based on negative feedback utilizes a non-intrusive control algorithm, hence minimizing complexity and expense. An MPPT system for ultra-low-power solar PV energy harvesting consists of a control system and a power converter [10].

However, this research doesn't use methods similar to Maximum Power Point Tracking (MPPT). Instead, our study concentrates on a solution that encompasses thorough testing and evaluation of the solar panel system's operational performance and efficiency across different load conditions. This approach yields valuable insights into the system's performance and efficiency. The innovation of this solution allows for thorough testing and assessment of the solar panel system's operational performance and efficiency under different load scenarios, offering valuable insights into its overall performance and efficiency.

The whole system operation procedure may be inferred from Figure 1. This diagram depicts the whole operational method of the solar panel power generating system, show-
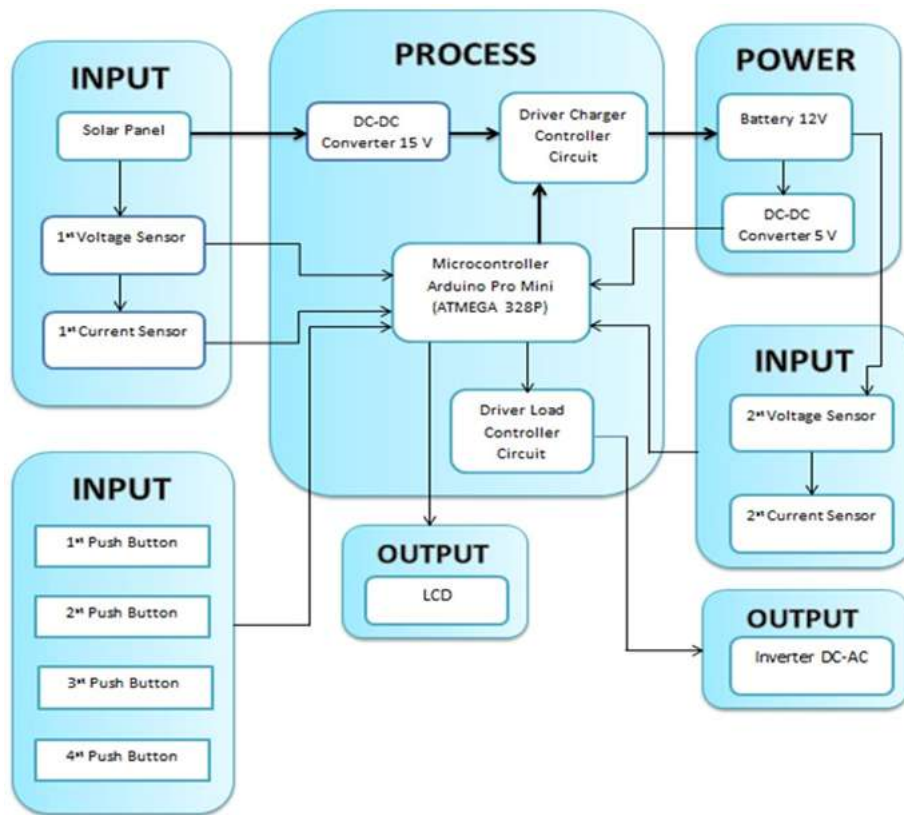
Figure 1: Block diagram.

casing the power, input, process, and output components. It offers a comprehensive explanation of the system's hardware architecture and functioning.

The system uses a secondary battery type, which means it can be charged back when the energy capacity has been exhausted. The battery used is 12 V with a capacity of 80 AH. The battery activates the microcontroller Atmega328P (Arduino Pro Mini 5 V 16 MHz), LCD, and Inverter DC – AC. The voltage required to enable the microcontroller Arduino Pro Mini and LCD is 5V, so the needed DC-DC Converter is 5 V (Step Down) to change the 12 V to 5 V.

Table 1 in this research presents a comprehensive summary of the application of alternative energy conversion through the utilization of solar panels and batteries for storage purposes. The crucial parameters of solar panels comprise rated voltage, capacity, discharge breaking voltage, limiting charging voltage, and battery charging-discharging technique.

There are multiple phases to the battery system on a solar panel. When the solar panel gets sunlight, solar energy is transformed into electric energy by the solar cell. This electric energy then flows into the battery to be stored [11–13].

Solar panel batteries are typically lithium-ion or lead-acid batteries. When electricity passes into the battery, the energy is charged and stored. As long as the solar panel receives sunlight, the battery will continue to charge [13].

Table 1: Battery specification

Item		Rated Performance	Note
Rated voltage		13.2 V	-
Discharge cut-off voltage		11.5 V	-
Rated capasity		80 Ah	-
Limited charge voltage		14.6 VDC	-
Charge method		CC-CV (Constant current with constant voltage)	-
Initial internal resistance		5.7 mΩ	-
Operating temperature:	Charge	$5°C \sim +60°C$	Humidity 65 $\pm$20%
	Discharge	$10°C \sim +60°C$	Humidity 65 $\pm$20%
Storage temperature	Standing	$10°C \sim +35°C$	Humidity 65 $\pm$20%
less than one year:	Storage		

When the sun does not shine or the electricity demand grows, it is possible to make use of the energy that has been stored in the battery [14]. The battery will discharge the stored energy to fulfill its electrical requirements. That energy enables stable and continuous electricity use without sunlight [15]. The batteries are capable of mitigating the issue of intermittency and delivering a consistent power source. In certain instances, the battery can store excess solar energy and sell it back to the power infrastructure [11].

2.2   Block Input

2.2.1   Solar panel

Solar panels are typically determined by solar radiation intensity. The sun undergoes diurnal motion, solar panels can collect more sunlight, boosting their output and increasing the amount of energy converted by up to 60 % [16].

The solar cell's structure is formed into a p-n junction, where the semiconductor substance providing it transforms light energy into direct current (DC) electricity via the photovoltaic effect [17]. It's made up of two types of semiconductors: one with an abundance of electron-hole pairs (n-type) and another with an abundance of holes (p-type) [18].

Physical Specification
- Model   : Solar Panel 50 W
- Cell Type   : Crystalline Silicon
- Operating Temperature   : $\sim$-20 ºC $\sim$ + 60ºC
- Max Power (Wp)   : 50W
- Max Voltage (Vmp)   : 18 V
- Max Current (Imp)   : 2.78 A
- Open Circuit Voltage (Voc)   : 21.5 V
- Short Circuit Current (Isc)   : 3.04 A
- Size (L x W)   : 63 x 48 x 1cm^2

Figure 2: Specification of solar panel.

When photons from sunlight produce electron-hole pairs in the depleted region of the junction, elevated electrons are sent to a load outside the cell through an electrical connection [19]. This process enables solar energy to be converted into electricity [19].

Figure 2 provides details on the specs of the solar panels that serve as the foundation for the design of the automated charging system. The maximum voltage (V_{mp}) is 18 V, which necessitates a voltage step-down mechanism capable of accommodating the battery being used, as batteries are limited to a range of 13 V to 14.6 V. The fill factor and efficiency of solar panels were

$$AFF = \frac{18V \times 2.78A}{21.5V \times 3.04A} = 0.77 \tag{1}$$

The input power for efficiency calculations is 1 kW/m2 or 100 mW/cm2. Thus, the input power for a (63×48) cm^2 panel is 302.4 W.

$$\eta = \frac{21.5\text{V} \times 3.04 \times 0.77}{302.4\text{W}} = 16.64\% \tag{2}$$

2.2.2 Voltage and current sensors

Voltage sensors measure the battery and solar panel voltages so the microcontroller can interpret them [20]. Furthermore, the voltage sensor in the battery is used as an indicator to determine the battery's status, allowing the charging procedure to be completed automatically [21]. The voltage sensor is designed to measure the electrical potential difference across the battery so that the microcontroller knows if the battery is full (voltage of battery > 13.2 V) or not.

Figure 3 illustrates the circuit configuration for the current sensor on the solar panel and battery, demonstrating the measurement and monitoring of the current used in the system. The present sensor employs Hall effect technology to eliminate the requirement of a shunt resistor and current transformer connected in series with the load. The small sensor incorporates a dynamic offset cancellation module, which is then amplified and filtered before being sent via pin 2. The module may be seamlessly incorporated into various systems and strategically positioned near the output of solar panels and batteries. The power supply is linked to pins 1 and 3, the microcontroller for solar panels is attached to pin 2, and the battery current calculator is connected to pin A7. Current sensors measure the current used in the system and are powered by solar panels, which may be seen on the LCD.

2.2.3 Push button

An analysis of characteristics and connections with subjective data collected from microcontroller systems enables the identification of issues in this particular study area, such as the importance of managing design variations for push buttons [22].

To configure the solar panel system, the microcontroller will be connected to the four buttons on the push button series. As seen in Figure 4, The button connected to the D12 pin is used to signal the status of the solar panel. The push buttons linked to D13 show the current state of the battery and the continuing charging process. The button associated with the D14 pin displays the present status (ON/OFF) and power level of the inverter battery. The push button connected to the D15 pin initiates and disables the inverter. Enabling push buttons by applying a logic level of HIGH (1).
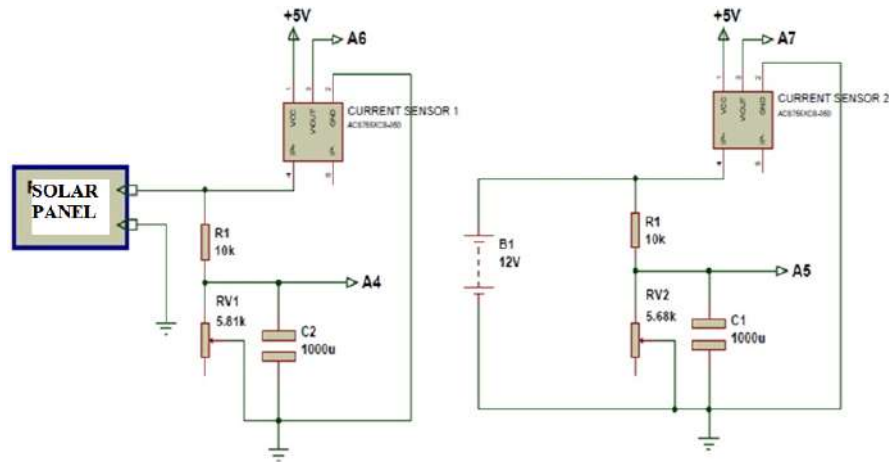
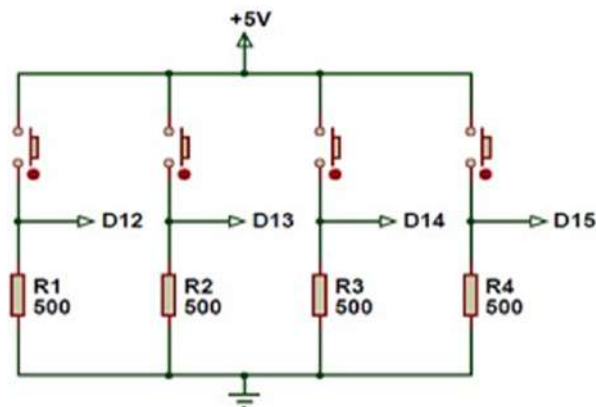Figure 3: Circuit current sensor on (a) solar panel (b) battery.

Figure 4: Push button circuit.

2.3 Block Process

2.3.1 Driver charger controller circuit and driver load controller

The driver circuit controller charges and manages loads using a p-channel mosfet and an NPN transistor. PWM signals are used to activate transistors used as switches.

The PWM signal is generated by a digital pin on the microcontroller (D3 and D10). The transistor works as a switch that works in cut-off mode and saturation. Figure 5 illustrates the process of constructing a driving circuit controller, charger, and load controller, using p-channel MOSFETs and NPN transistors. The transistors are activated by a PWM signal generated by two digital pins (D3 and D10) on the microcontroller. The transistor operates in both saturation and cut-off states. The Driver Charge Controller circuit is activated as shown in Figure 5 using a PWM signal with duty cycle values of 255, 218, 128, and 0. The
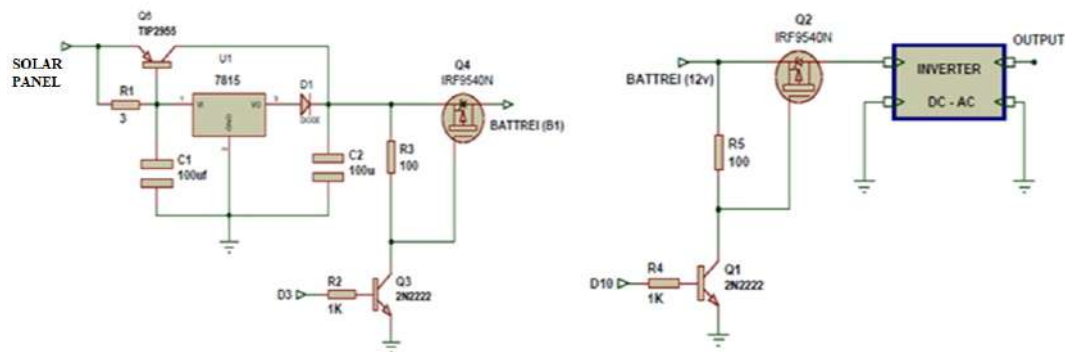
Figure 5: (a) Driver charge controller (b) Driver load controller circuits.

microcontroller may generate the PWM signal by using the instruction (PWM, Duty cycle value).

2.3.2 Microcontroller

The microcontroller was Arduino Pro Mini 16 MHz (Atmega328P 32 pin). The microcontroller is used as the control center of this system both in the automatic charging process and in giving the desired output [23]. The minimum system on the microcontroller can be seen in Figure 6.

Figure 6 illustrates the microcontroller's interaction with several pins, namely D9, D2, D4, D5, D6, D6, D9, D10, and D11. The Arduino Pro Mini 16MHz microcontroller functions as the core component of an automated charging system. The sensor's output voltage is quantified as 2.5 V and fluctuates at intervals of 100 mV, with 1 A being regarded as the ideal amount. The goal of this data is to expedite the execution of microcontroller programming algorithms that assess the electrical current produced by solar panels and batteries.

Pins A0, A1, A2, A3, A4, A5, A6, and A7 on the Arduino Pro mini can be set up for analog input. One analog pin is used by the voltage and current sensors on the battery and solar panel to detect the generated voltage [24]. Every analog input is converted to a digital value with 10 bits.

Figure 7 provides the information that should be observed. PWM output can be configured on pins D3, D5, D6, D9, D10, and D11. PWM signals are generated via pins D3 and D10 by the charging mechanism, with pin D3 being controlled by Timer/Counter Control Register 0A (TCCR0A). The default PWM signal operates at a frequency of 490.20 Hz and has a 64 prescaler. The device functions in the Fast PWM mode, more precisely in the Non-inverting mode.

2.4 Block Output

2.4.1 LCD

LCDs the status and condition of solar panels and batteries [25]. This section uses LCDs with a 16 × 2 aspect ratio, indicating 16 columns and two rows [26]. Pins D2, D9, D4, D5,
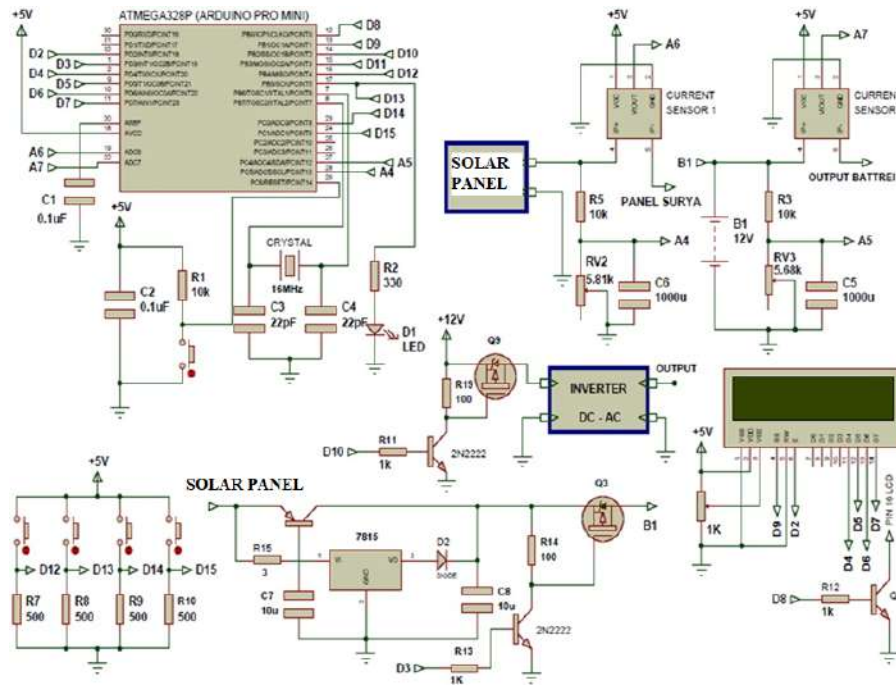
Figure 6: Minimum system microcontroller arduino pro mini (Atmega 328P).

D6, and D7 of the microcontroller are connected to this LCD. Figure 8 displays an LCD circuit.

The LCD supply voltage is 5 V, and the brightness of the LCD can be adjusted to modify the incoming voltage at pin 3 of the LCD [27]. To modify the voltage on pin 3, use a voltage divider 1k. This LCD is controlled by three pins: RS (Register Select), RW (Read / Write selection), and E (Enable).

2.4.2 Inverter

While on the driver, the power amplifier consists of a transistor circuit Collector Feedback and a pair of feedback-equipped power amplifiers [28]. Figure 9 displays the inverter's block diagram.

Figure 9 displays the block diagram of the inverter, which emphasizes the sinusoidal wave generator and power amplifier driver component. This document offers a comprehensive description of the design and components of the inverter system.

The inverter is separated into two key sections in this research: a sinusoidal wave generator and a power amplifier driver component. The sinusoidal wave generator was made up of four steps: a square wave generator using an astable multivibrator IC 555, a phase divider using IC 74LS04, a low pass filter, and a non-inverting amplifier.
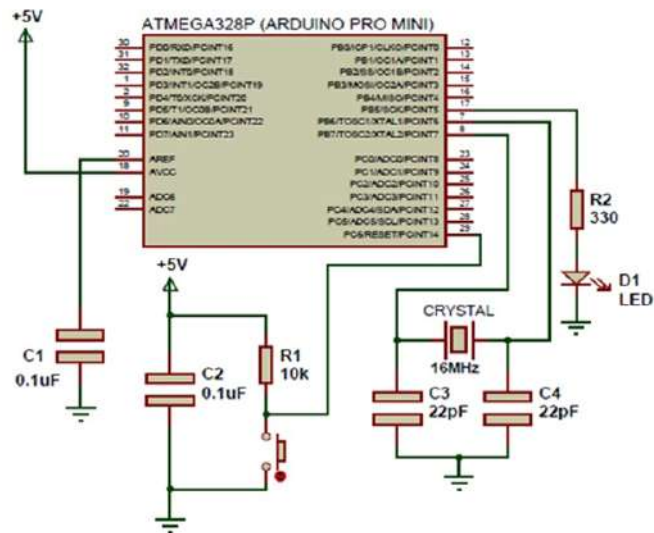
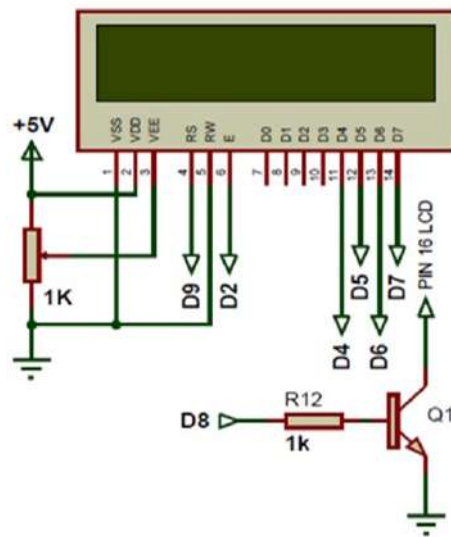Figure 7: Circuit overall at microcontroller arduino pro mini.
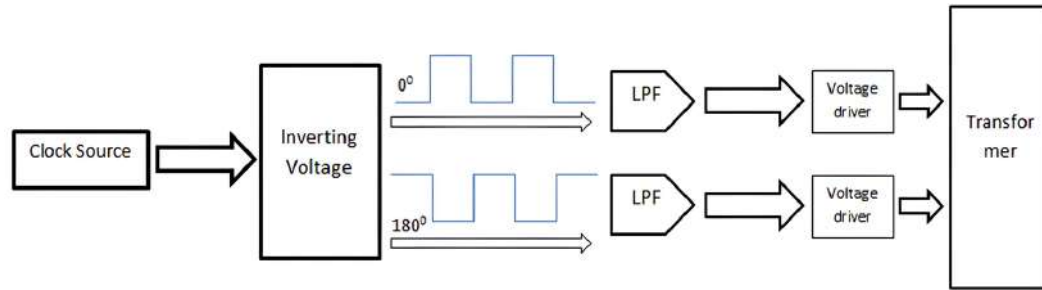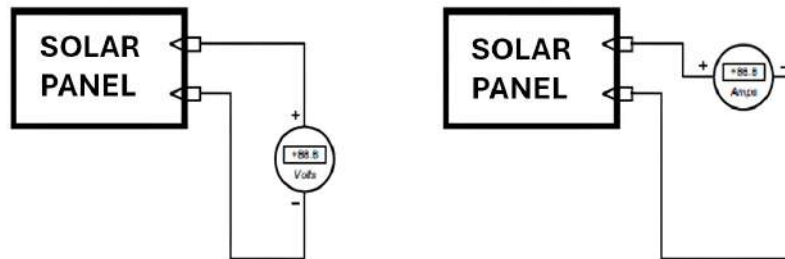

Figure 8: LCD circuits.

Figure 9: Block diagram inverter.

3 Results

3.1 Testing of Solar Panel

the solar panel's open-circuit voltage (V_{OC}) and short-circuit current (I_{SC}) are obtained in sunshine to test solar panels. The data was collected from 07.00 a.m. to 05.00 p.m. and making observations every 30 minutes.

Figure 10: Schematic of measurement solar panel (a) V_{OC} and (b) I_{SC}.

According to Figure 10, the diagram illustrates the measurement of V_{OC} and I_{SC}. The provided graphic illustrates the diagram of the measuring arrangement for the solar panel, specifically demonstrating the measurements of V_{OC} and I_{SC}. It offers valuable information about the testing procedure for the solar panel system.

Assign varying durations to V_{OC} and I_{SC} measurements to assess the solar panel system's ability to convert the energy presented in Table 2 into usable power. Based on the measurement results in Table 2, V_{OC} is 21.06 V, reached at midnight. When compared with the specifications of the solar panels that are used, the:

$$\text{Achievement of } V_{OC} = \frac{\text{Max } V_{OC}}{V_{OC} \text{ on specs}} \times 100\%$$
$$= \frac{21.06}{21.50} \times 100\% = 97,95\%$$

(3)

2Time (WIB)l	First Day		Second Day		Third Day	
	V_{OC}(V)	I_{SC}(A)	V_{OC}(V)	I_{SC}(A)	V_{OC}(V)	I_{SC}(A)
07.00	19.46	0.35	19.36	0.30	19.50	0.39
07.30	19.59	0.41	19.40	0.32	19.60	0.43
08.00	20.88	1.40	19.46	0.35	19.79	0.46
08.30	20.33	1.83	19.41	0.34	20.30	1.80
09.00	20.53	**2.25**	19.36	0.30	19.50	0.39
09.30	20.01	1.75	19.59	0.41	20.23	1.90
10.00	20.02	2.12	19.69	0.53	20.46	**2.07**
10.30	20.04	2.18	19.55	0.49	20.53	1.56
11.00	20.07	2.21	19.45	0.45	20.60	1.39
11.30	20.66	1.66	19.57	0.50	20.76	1.83
12.00	**21.06**	2.00	18.76	0.24	20.87	1.70
12.30	20.26	1.54	16.20	0.06	**21.01**	1.89
13.00	20.36	1.16	0	0	20.97	1.59
13.30	20.45	1.65	0	0	20.39	1.17
14.00	20.05	1.28	0	0	19.79	1.06
14.30	19.88	0.54	**19.85**	**1.19**	19.98	0.90
15.00	19.63	0.54	**19.85**	**1.19**	19.98	0.90
15.30	19.72	0.58	19.75	1.09	19.88	0.85
16.00	19.55	0.49	18.76	0.24	19.40	0.38
16.30	19.50	0.40	18.49	0.30	19.59	0.55
17.00	18.88	0.25	18.60	0.32	17.80	0.09

Table 2: Measurement of solar panel in Depok at (25- $40°$ C)

The measured value of the V_{OC} on the solar panel is 21.06 V or reaches 97.95 % of the maximum desired V_{OC}. The I_{SC} is the highest obtained from measurements was 2.25 A, occurred at 09.00 a.m. When compared with the specifications of the solar panels, then:

$$\text{Achievement of } I_{SC} = \frac{\text{Max } I_{SC}}{I_{SC} \text{ on specs}} \times 100\%$$
$$= \frac{2.25}{3.04} \times 100\% = 74.01\%$$

(4)

Based on the results in (4), the measurement of solar panels that obtained short circuit current reaches 74.01 % of the maximum desired I_{SC}. From the data V_{OC} and I_{SC} generated by the solar panel, the maximum power (P_m) generated by the solar panels can be known:

$$FF = \frac{P_m}{V_{OC} \, I_{SC}}$$
$$P_m = V_{OC} \times I_{SC} \times FF$$
$$= 20.53V \times 2.25A \times 0.77 = 35.57W$$

(5)

According to the measurements shown in Table 2, Figure 11 illustrates a chart depicting the V_{OC}. The highest recorded voltage is 21.06 V, which occurred precisely at 12.00 a.m. The maximum power generated from the measurement was 35.57 W, which occurred on the first day of testing at 09.00 a.m.
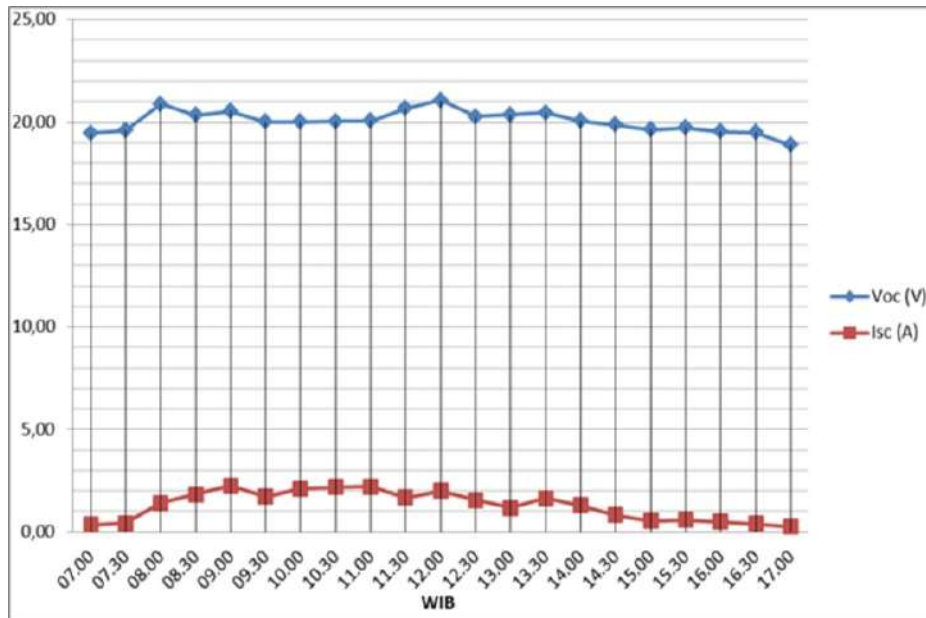
Figure 11: Graph of V_{OC} and I_{SC} on first day.

3.2 Testing the Battery Voltage

Figure 12 (a) shows that when solar panels are used as a power source and attached to the DC-DC step-down converter, there is no current flow. This is because the battery is badly damaged, as shown by the 6.10 V voltage reading. When the battery in Figure 12 (b) is used, current from the solar panels can flow into the battery.

Figure 12: Results of testing battery condition (a) bad and (b) good enough.

3.3 Testing of DC-DC Step Down Converter

This battery requires a DC voltage more significant than 13 V but not greater than 14.6 V to charge. So that the output of IC 7815 is provided with a diode that can reduce the voltage

without converting the current into heat, as would be the case with a resistor-based voltage divider.

Figure 13: Measurement DC-DC step down converter.

Figure 13 shows that the measurement result is 14.52 V, which is already eligible for charging the battery because it does not exceed 14.6 V.

3.4   Test DC-DC Step-Down Converter Efficiency

Efficiency testing is done by measuring the voltage (V_1 and V_2) and the current (I_1 and I_2) or when the circuit is connected to the solar panels and the load on the battery. Figure 14 shows the scheme for the tests.
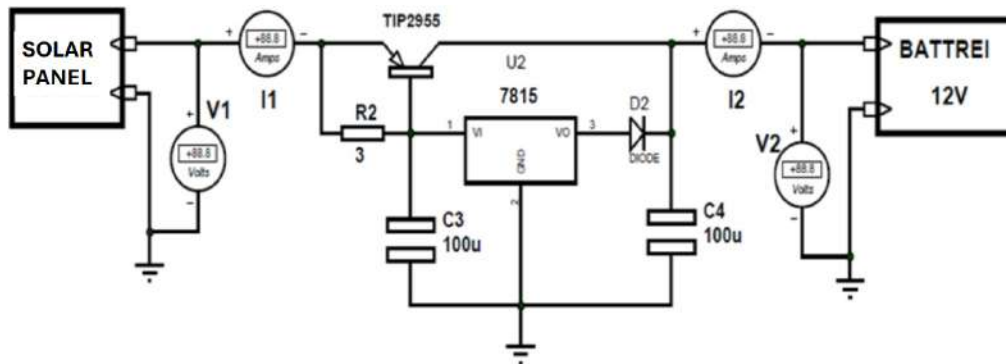

Figure 14: Scheme of testing V_1, V_2, I_1, and I_2.

After measuring the V_{OC} and I_{SC} that solar panels can generate, test the voltage and current when it is connected to the load to determine the efficiency of a step-down converter circuit. The measurement data are presented in Table 3.

Table 3 of this paper presents additional information regarding the operational performance and efficiency of the solar panel system under load conditions, derived from the testing data acquired for the system. The data includes current measurements (I_1 and I_2)

Table 3: Measurement data V_1, V_2, I_1, and I_2

2Time (WIB)l	First Day			
	V_1(V)	V_2(A)	I_1(V)	I_2(A)
07.00	14.82	11.90	0.32	0.29
07.30	14.90	11.39	0.38	0.35
08.00	15.80	12.59	1.37	1.36
08.30	15.66	12.62	1.8	1.5
09.00	16.38	13.08	2.21	2.1
09.30	15.51	12.51	1.5	1.45
10.00	15.38	12.45	2.08	2.08
10.30	15.56	12.53	2.16	2.15
11.00	15.37	12.34	2.2	2.2
11.30	15.16	12.16	1.44	1.4
12.00	15.50	12.50	1.98	1.94
12.30	15.44	12.44	1.26	1.22
13.00	15.28	12.18	1.08	1.04
13.30	15.34	12.34	1.26	1.22
14.00	15.89	12.80	1.15	1.1
14.30	15.04	12.09	0.77	0.69
15.00	14.38	12.01	0.54	0.48
15.30	14.39	12.04	0.58	0.56
16.00	14.91	11.98	0.48	0.42
16.30	14.86	11.90	0.34	0.30
17.00	14.10	11.82	0.21	0.20

and voltage measurements (V_1 and V_2) at different time intervals. A comparison of the testing outcomes with those of the prior investigation allows for an assessment of the load's impact on the voltage and current properties of the system, thereby facilitating an evaluation of its stability, power output, and overall performance.

The measurement results of the average currents in I1 were 1.1967 A, and the average currents in I2 was 1.1467 A. Thus, the known efficiency of a step-down converter can be seen in (1).

$$\text{Efficiency} = |\frac{Average\ T_2}{Average\ T_1}| \times 100\%$$
$$= |\frac{1.1467}{1.1967}| \times 100\% = 95.81\%$$
(6)

So that the efficiency is 95.81 %, meaning that the current from the solar panels will be distributed to the battery well. If in one day, the average current flowing into the battery was 1.15 A and from measurements in two days the battery is charged 18 %, then to fill the battery with 80 Ah capacity takes time.

$$\text{Average time charging} = \frac{80\ Ah}{1.15\ A} = \pm 69.56\ hours$$
(7)

If a day's best time is 08.00 a.m. to 03.00 p.m., from empty to fully charged battery takes $\pm$ 10 days.

3.5   Testing Automatic Charging with PWM System

To know whether the automatic charging works well, then do the testing using an oscilloscope to know the PWM generated by a microcontroller. The circuit testing procedure is displayed in Figure 15.
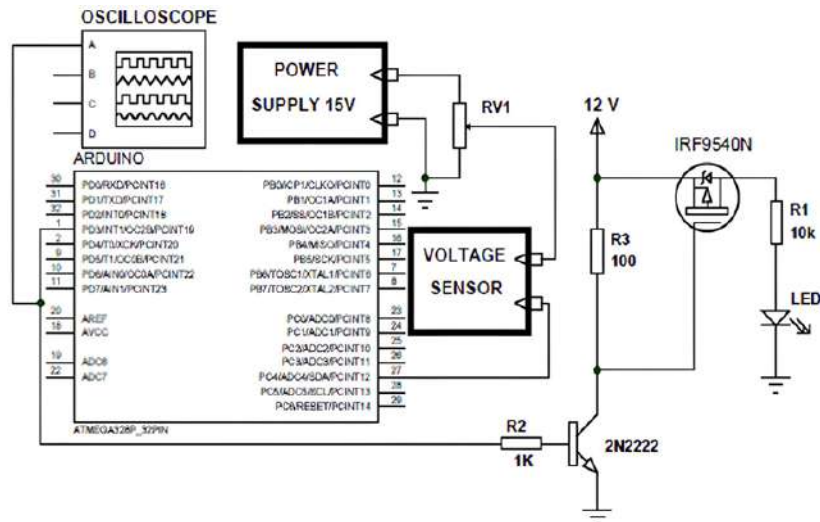

Figure 15: Circuit testing of automatic charging.

Figure 15 explains the process of testing the circuitry of an automatic charging system. The provided image displays the experimental arrangement for evaluating the automatic charging system utilizing a PWM system. The setup comprises the microcontroller and the components necessary for the automated charging process.

The test results are shown in Figure 16, Figure 17, Figure 18, Figure 19, and Figure 20. Figure 16 shows a stand-by condition, which refers to a state in the system where there is neither charging nor discharging occurring, resulting in the PWM output being turned off. The battery level is currently at 19 %, which falls under the range of less than 25 %. The charging process can be initiated, causing the PWM to activate with a duty cycle of 255, as depicted in Figure 17. Figure 18 displays the battery condition at 45 %, falling within the range of 25 % to less than 75 % which categorizes it. Therefore, the charging process will be initiated and the PWM will be activated with a duty cycle of 218.

Figure 19 displays the battery's current condition, which is at 81 %. The battery falls within the group of 75 % or greater but less than 100 % in terms of its status. Therefore, the charging process will commence and the PWM will be activated with a duty cycle of 128. According to Figure 20, the battery status is at 100 % and falls into the 100 % group. The charging mechanism is currently deactivated and the PWM will also be deactivated, resulting in a duty cycle of 0.
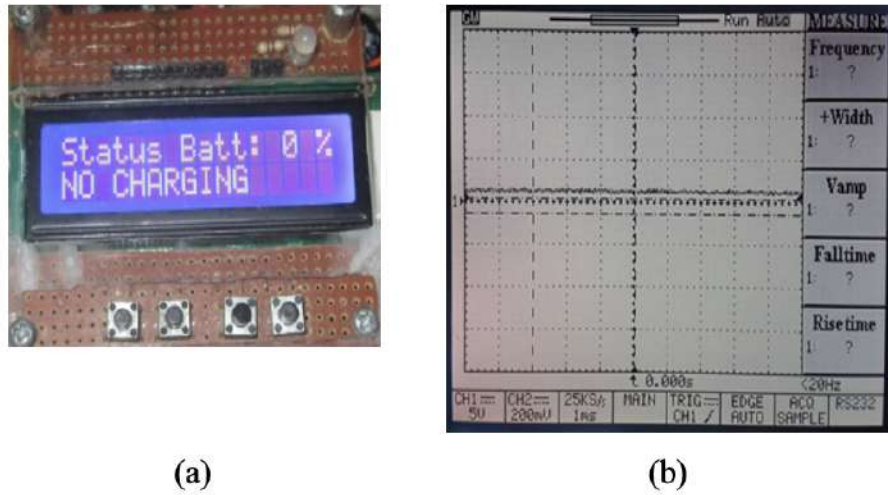
Figure 16: Automatic charging testing results With PWM in standby condition (a) LCD status (b) signal PWM.
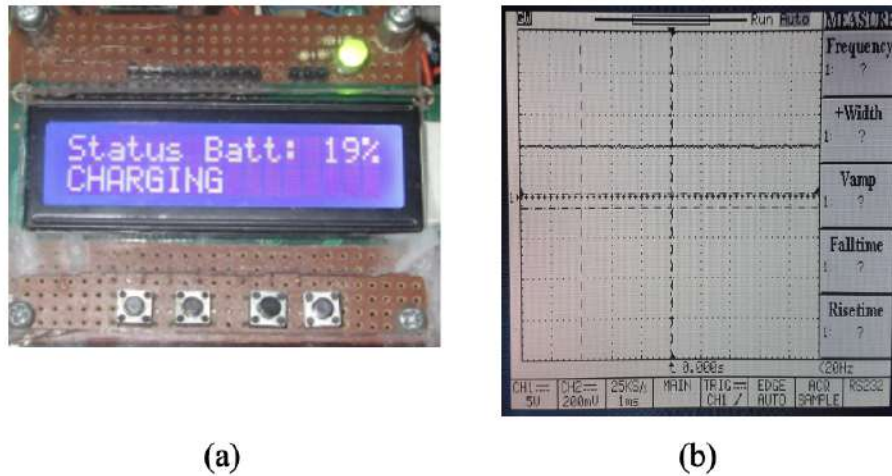

Figure 17: Automatic charging testing results with PWM in status of battery condition < 35 % (a) LCD status (b) signal PWM.

3.6 Inverter Testing

3.6.1 Square wave generator

The desired output of IC 555 is a square wave with a frequency ranging from 50 to 60 Hz. As depicted in Figure 21, the square wave exhibited a period (T) of 20.00 ms, which can be calculated using (8).
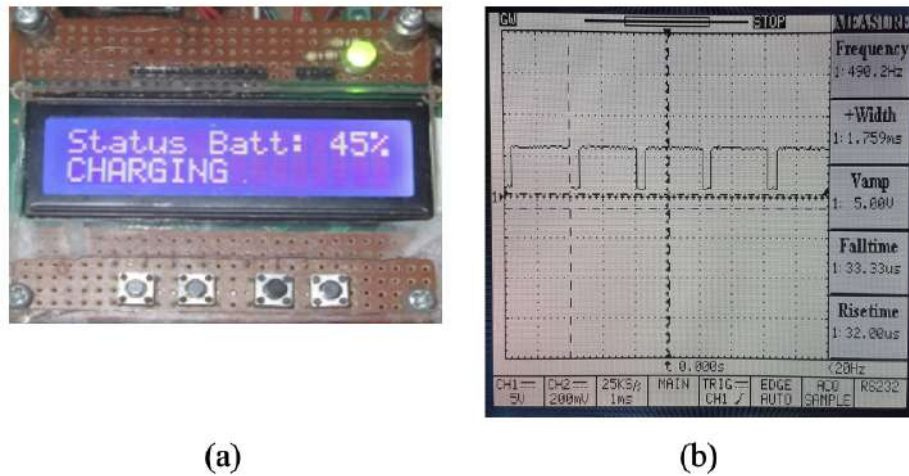
(a)   (b)

Figure 18: Automatic charging testing results with PWM in 25 % ≤ status of battery < 75 % condition (a) LCD status (b) signal PWM.
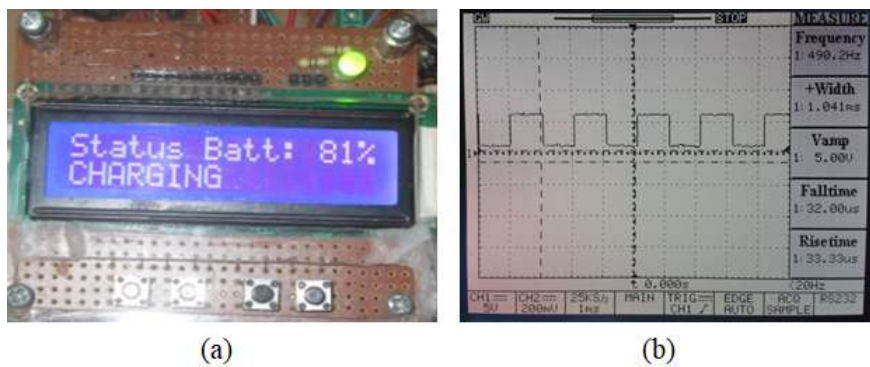

(a)   (b)

Figure 19: Automatic charging testing results with PWM in 75 % ≤ status of battery < 100 % condition (a) LCD status (b) signal PWM.

$$f = \frac{1}{r}f = \frac{1}{20 \times 10^{(-3)}} = 50Hz \tag{8}$$

The resulting frequency is 50 Hz, which matches the needed specifications. The utilization of IC 74LS04 results in the production of a signal oscillating at a frequency of 50 Hz, accompanied by a phase shift of $180°$.

Figure 21 represents the many stages of the square wave generator, offering a glimpse into the waveform produced by the system's square wave generator during testing.
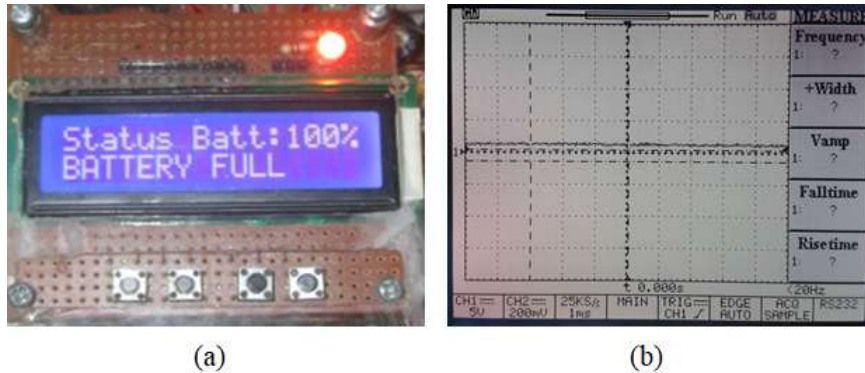
Figure 20: Automatic charging testing results with PWM in status of battery 100 % condition (a) LCD status (b) signal PWM.
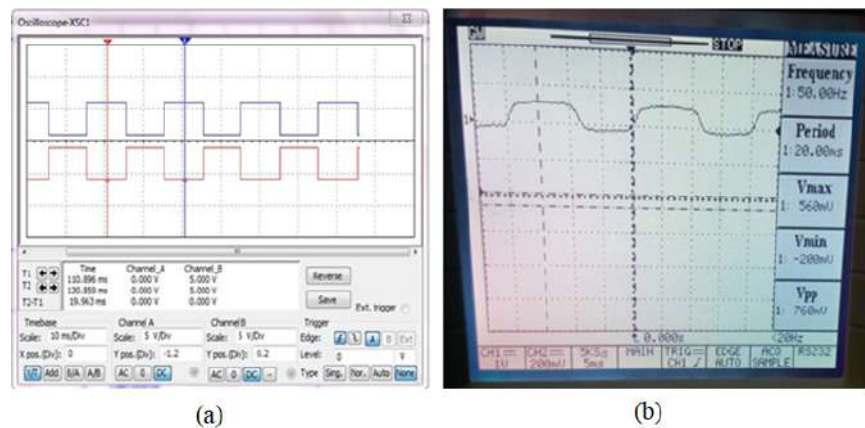

Figure 21: Square wave different phase 1800 (a) simulation results (b) hardware result.

3.6.2 Low pass filter and non-inverting amplifier

The non-inverting amplifier will enhance the output of the low pass filter. The input square wave of IC 555 has been transformed into a sinusoidal wave with the implementation of a low-pass filter.

Figure 22 (b) shows that the output signal has a period (T) of 19.00 ms, which indicates a frequency difference of 5.26 % from the input frequency, equivalent to 52.63 Hz. However, the frequency range that is still considered acceptable is between 50 and 60 Hz. The non-inverting amplifier will strengthen the output of the low pass filter. Results of low pass filter: the input square wave of IC 555 has been changed into a sinusoidal wave.
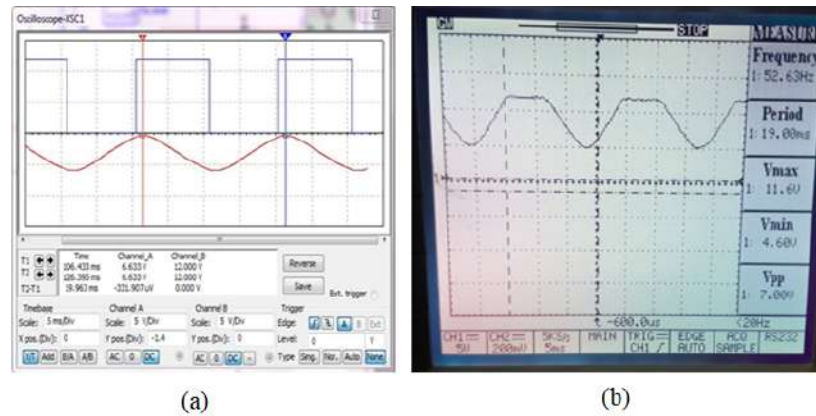
Figure 22: Results sinusoidal wave of low pass filter.

3.6.3 Output signal of feedback collector amplifier

As seen in Figure 23, the result output signal of the amplifier has a different phase 180o from the input signal. Because the V_{cc} input to the Feedback Collector Amplifier is 12 Volts, the expected gain from the system is 12 V_{pp}. So, that the system test results are obtained in (9).

$$\begin{aligned} \text{Error rate} &= \frac{\text{Strengthening desired} - \text{Strengthening testing}}{\text{Strengthening desired}} \times 100\% \\ &= \frac{12V_{pp} - 20.4V_{pp}}{12V_{pp}} \times 100\% \\ &= 13.33\% \end{aligned} \tag{9}$$
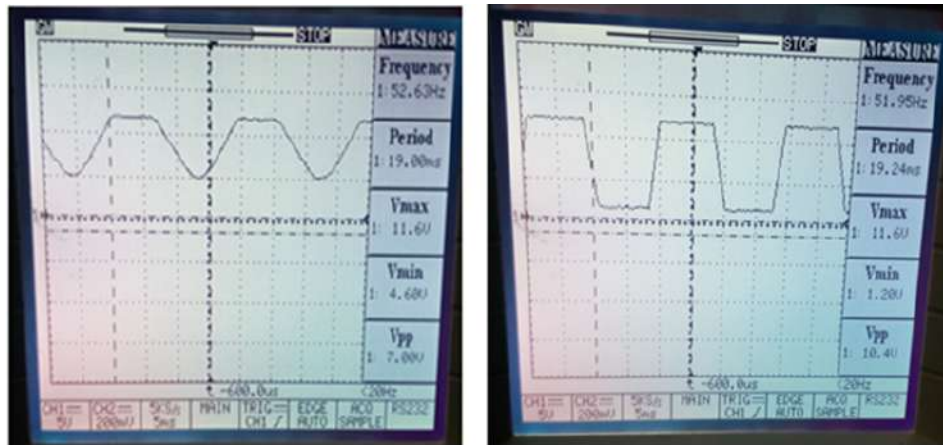
3.6.4 Output signal of pair feedback amplifier

The output signal of the pair feedback amplifier is depicted in Figure 24. In the figure, the collector input voltage of the feedback amplifier measures 10.4 Volts. The magnitude of the feedback voltage is 10.6 Volts peak-to-peak. The average value (Av) throughout device design is 1.45, which leads to an error rate of 29.71 %. The voltage transformers will provide a connection between the final output of the amplifier.

The output of the transformer is shown in Figure 25. The figure demonstrates that the final output of the inverter is 193.6 V_{ac}, so the error rate of the inverter is shown in (10).

$$\text{Error rate} = \frac{220V_{ac} - 193.6V_{ac}}{220V_c} \times 100\% = 12\% \tag{10}$$

Figure 26 illustrates the procedure of collecting data for solar panels and testing the inverter with a load. This document offers a comprehensive outline of the testing procedure and data gathering for the solar panel power generating system.

(a)   (b)

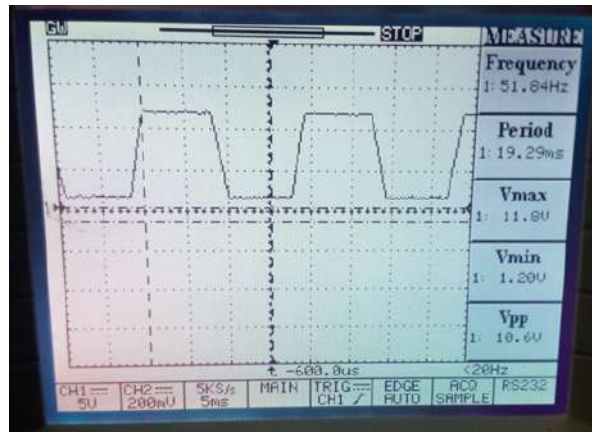Figure 23: Results of testing output signal (a) non-inverting amplifier (b) feedback collector amplifier.

Figure 24: Output signal of pair feedback amplifier.

Table 4 displays the results of testing for a solar panel system connected to a load, evaluating performance and efficiency. When these data are compared to earlier findings, it is possible to examine the impact of load on the system's voltage and current characteristics, as well as its stability, power output, and overall performance. In general, the battery specifications, solar panel measurements, and load testing data offer significant insights into the performance and efficiency of the solar panel system.

Figure 25: Output of voltage transformer 500 mA.

Figure 26: Process testing systems overall.

4 Discussion

PWM and maximum power point tracking (MPPT) are the prevailing types of controllers employed in contemporary solar power systems [29]. It modulates the charging pace based on the battery's charge level to optimize the charge towards the battery's full capacity, while also monitoring the battery voltage to prevent excessive charging [30]. When charging a battery using a solar panel, several aspects need to be taken into account. If the sole criterion for selecting a solar controller was to maximize charging capacity, then MPPT controllers would be universally preferred over PWM controllers [31]. Nevertheless, the two

Table 4: Testing using load

No	Light	Condition
1	5 W	Bright
2	7 W	Dim

technologies diverge and possess distinct benefits. The determination relies on factors such as site conditions, system components, array size, and load, with the ultimate consideration being the cost of a certain solar power system.

5 Conclusion

The research achieved the development of a solar panel power generator with automatic charging using a PWM system based on a microcontroller. It involved hardware design, testing of solar panel measurements, and the design and testing of a solar energy system using solar panels, batteries, and inverters. The results showed that the open-circuit voltage (VOC) reached 97.95 % of the maximum desired value, the short circuit current (ISC) reached 74.01 % of the maximum desired value, and the maximum power generated from the solar panels was 35.57 W. The DC-DC step-down converter was additionally determined to have an efficacy of 95.81 %. Ten days were estimated to be the time required to completely charge a battery with an 80 Ah capacity. Testing was performed on the automatic charging with the PWM system, as well as on the inverter. The objective of the research was to use solar light energy as an alternative source of energy to decrease reliance on oil and gas. The study also presented findings regarding the system's power generating and charging capacities, along with suggestions for enhancing its efficiency.

Table 5: Comparative analysis of current and previous research findings

Ref	[1]	[2]	[3]	[This Work]
Method	Perturb and Observe (P and O) algorithm for with a buck-boost charge controller.	Improved incremental conductance algorithm.	Improved conventional Fractional Open Circuit Voltage (FOCV) method.	Microcontroller and PWM.
Feature	-	Duty cycle adjustment to operate at the maximum power point (MPP) and maintains photovoltaic voltage.	-	DC-DC step-down converter, CC-CV charging method, and PWM control
Result	• More stable and accurate. • Increased tracking speed by 20 % to 30 % for different irradiance variation ranges. • Improved response time.	• System performance under varying weather and loading conditions enhanced. • Effectively estimates Vmpp under different irradiance values.	• Accurately estimate maximum power point voltage.	• VOC of solar panels reached 97.95 % of maximum desired value. • ISC achieved 74.01 % of maximum desired value. • DC-DC step-down converter efficiency was 95.81 %.

Acknowledgments

References

[1] M. B. Hayat, D. Ali, K. C. Monyake, L. Alagha, and N. Ahmed, "Solar energy - A look into power generation, challenges, and a solar-powered future," *Int J Energy Res*, vol. 43, no. 3, pp. 1049–1067, Mar. 2019, doi: 10.1002/er.4252.

https://ejournal.ittelkom-pwt.ac.id/index.php/infotel

[2] B. S. Aprillia, I. M. H. Keswara, J. Raharjo, M. Ramdhani, K. B. Adam, and E. Suhartono, "Standalone photovoltaic system cost optimization for Matantimali village Central Sulawesi," *IOP Conf Ser Mater Sci Eng*, vol. 982, no. 1, p. 012023, Dec. 2020, doi: 10.1088/1757-899X/982/1/012023.

[3] B. S. Aprillia and M. A. F. Rigoursyah, "Design on-grid solar power system for 450 VA conventional housing using HOMER software," *IOP Conf Ser Mater Sci Eng*, vol. 771, no. 1, p. 012011, Mar. 2020, doi: 10.1088/1757-899X/771/1/012011.

[4] Ministry of Energy and Mineral Resources Republic of Indonesia, "Indonesia's effort to phase out and rationalise its fossil-fuel subsidies (A self-report on the G-20 peer review of inefficient fossil fuel subsidies that encourage wasteful consumption in Indonesia)," Osaka, Jun. 2019. Accessed: Oct. 31, 2023. [Online]. Available: https://www.oecd.org/fossil-fuels/publication/Indonesia%20G20%20Self-Report%20IFFS.pdf

[5] PLN, "Tarif Adjustment." Accessed: Oct. 31, 2023. [Online]. Available: https://web.pln.co.id/statics/uploads/2017/06/TA-Desember-2016.jpg

[6] D. F. Silalahi, A. Blakers, M. Stocks, B. Lu, C. Cheng, and L. Hayes, "Indonesia's vast solar energy potential," *Energies*, vol. 14, no. 17, p. 5424, Aug. 2021, doi: 10.3390/en14175424.

[7] D. Baimel, S. Tapuchi, Y. Levron, and J. Belikov, "Improved fractional open circuit voltage MPPT methods for PV systems," *Electronics*, vol. 8, no. 3, Mar. 2019, doi: 10.3390/electronics8030321.

[8] L. Shang, H. Guo, and W. Zhu, "An improved MPPT control strategy based on incremental conductance algorithm," *Protection and Control of Modern Power Systems*, vol. 5, no. 1, Dec. 2020, doi: 10.1186/s41601-020-00161-z.

[9] V. Bhan, S. A. Shaikh, Z. H. Khand, T. Ahmed, L. A. Khan, F. A. Chachar, and A. M. Shaikh, "Performance evaluation of perturb and observe algorithm for MPPT with buck–boost charge controller in photovoltaic systems," *Journal of Control, Automation and Electrical Systems*, vol. 32, no. 6, pp. 1652–1662, Dec. 2021, doi: 10.1007/s40313-021-00781-2.

[10] F. F. Ahmad, C. Ghenai, and M. Bettayeb, "Maximum power point tracking and photovoltaic energy harvesting for Internet of Things: A comprehensive review," *Sustainable Energy Technologies and Assessments*, vol. 47, Oct. 01, 2021. doi: 10.1016/j.seta.2021.101430.

[11] A. G. Olabi, T. Wilberforce, E. T. Sayed, A. G. Abo-Khalil, H. M. Maghrabie, K. Elsaid, and M. A. Abdelkareem, "Battery energy storage systems and SWOT (strengths, weakness, opportunities, and threats) analysis of batteries in power transmission," *Energy*, vol. 254, p. 123987, Sep. 2022, doi: 10.1016/j.energy.2022.123987.

[12] P. K. Pathak and A. R. Gupta, "Battery energy storage system," in *2018 4th International Conference on Computational Intelligence & Communication Technology (CICT)*, IEEE, Feb. 2018, pp. 1–9. doi: 10.1109/CIACT.2018.8480377.

[13] S. Shukir, "Solar energy batteries - A critical review," May 2022.

[14] R. Borah, F. R. Hughson, J. Johnston, and T. Nann, "On battery materials and methods," *Mater Today Adv*, vol. 6, p. 100046, Jun. 2020, doi: 10.1016/j.mtadv.2019.100046.

[15] J. Mitali, S. Dhinakaran, and A. A. Mohamad, "Energy storage systems: A review," *Energy Storage and Saving*, vol. 1, no. 3, pp. 166–216, Sep. 2022, doi: 10.1016/j.enss.2022.07.002.

[16] B. S. Aprilia, M. Z. Romdlony, J. Raharjo, and Y. G. Sidik, "Fuzzy based sensorless tracking controller on the dual-axis PV panel for optimizing the power production," *JURNAL INFOTEL*, vol. 13, no. 4, pp. 230–238, Dec. 2021, doi: 10.20895/infotel.v13i4.738.

[17] A. A. Bayod-Rújula, "Solar photovoltaics (PV)," in *Solar Hydrogen Production, Processes, Systems and Technologies*, 2019, pp. 237–295. doi: 10.1016/B978-0-12-814853-2.00008-4.

[18] M. H. Futscher, T. Schultz, J. Frisch, M. Ralaiarisoa, E. Metwalli, M. V. Nardi, P. Müller-Buschbaum, and N. Koch, "Electronic properties of hybrid organic/inorganic semiconductor pn-junctions," *Journal of Physics: Condensed Matter*, vol. 31, no. 6, p. 064002, Feb. 2019, doi: 10.1088/1361-648X/aaf310.

[19] S. Kim, V. Q. Hoang, and C. W. Bark, "Silicon-based technologies for flexible photovoltaic (PV) devices: From basic mechanism to manufacturing technologies," *Nanomaterials*, vol. 11, no. 11, p. 2944, Nov. 2021, doi: 10.3390/nano11112944.

[20] S. A. Jumaat, M. N. A. M. Said, and C. R. A. Jawa, "Dual axis solar tracker with IoT monitoring system using arduino," *International Journal of Power Electronics and Drive Systems (IJPEDS)*, vol. 11, no. 1, p. 451, Mar. 2020, doi: 10.11591/ijpeds.v11.i1.pp451-458.

[21] K. Song, D. Hu, Y. Tong, and X. Yue, "Remaining life prediction of lithium-ion batteries based on health management: A review," *J Energy Storage*, vol. 57, p. 106193, Jan. 2023, doi: 10.1016/j.est.2022.106193.

[22] N. Valverde, A. M. R. Ribeiro, E. Henriques, and M. Fontul, "An engineering perspective on the quality of the automotive push-buttons' haptic feedback in optimal and suboptimal interactions," *Journal of Engineering Design*, vol. 30, no. 8–9, pp. 336–367, Sep. 2019, doi: 10.1080/09544828.2019.1656802.

[23] A. Shufian, Md. R. Haider, and Md. Hasibuzzaman, "Results of a simulation to propose an automated irrigation & monitoring system in crop production using fast charging & solar charge controller," *Clean Eng Technol*, vol. 4, p. 100165, Oct. 2021, doi: 10.1016/j.clet.2021.100165.

[24] B. Al Kindhi, J. Pramudijanto, I. S. Pratama, L. P. Rahayu, F. I. Adhim, and J. Susila, "Solar cell based integrated sensor system monitoring on smart IoT," in *2021 IEEE International Conference on Communication, Networks and Satellite (COMNETSAT)*, IEEE, Jul. 2021, pp. 213–218. doi: 10.1109/COMNETSAT53002.2021.9530801.

[25] N. S. S. Mohamed, N. FaezahBintiAbdGhani, and N. F. A. Hamid, "Battery monitoring for stand-alone photovoltaic system," *J Phys Conf Ser*, vol. 1432, no. 1, p. 012054, Jan. 2020, doi: 10.1088/1742-6596/1432/1/012054.

[26] C-W. Lu, P-Y. L. Lee, Y-G. Chang, X-W. Huang, J-S. Cheng, P-Y. Tseng, C-H. Chou, P. Chen, T-Y. Chang, J. Y-C. Liu "A 10-bit 1026-channel column driver IC with partially segmented piecewise linear digital-to-analog converters for UHD TFT-LCDs with one billion color display," *IEEE J Solid-State Circuits*, vol. 54, no. 10, pp. 2703–2716, Oct. 2019, doi: 10.1109/JSSC.2019.2927444.

[27] D. K. Mahanta and I. Rahman, "IoT based transformer oil moisture monitoring system," in *2022 IEEE Delhi Section Conference (DELCON)*, IEEE, Feb. 2022, pp. 1–4. doi: 10.1109/DELCON54057.2022.9752870.

[28] S. M. Sharroush, "Design of the CMOS inverter-based amplifier: A quantitative approach," *International Journal of Circuit Theory and Applications*, vol. 47, no. 7, pp. 1006–1036, Jul. 2019, doi: 10.1002/cta.2628.

[29] M. R. Dhotre and P. V. Thakre, "Modeling of maximum power point tracking based photovoltaic open loop flyback inverter using sinusoidal pulse width modulation technique for performance improvement," in *2022 Second International Conference on Advances in Electrical, Computing, Communication and Sustainable Technologies (ICAECT)*, IEEE, Apr. 2022, pp. 1–6. doi: 10.1109/ICAECT54875.2022.9807918.

[30] B. Bose, A. Garg, B. K. Panigrahi, and J. Kim, "Study on li-ion battery fast charging strategies: Review, challenges and proposed charging framework," *J Energy Storage*, vol. 55, p. 105507, Nov. 2022, doi: 10.1016/j.est.2022.105507.

[31] Y. A. Jieb and E. Hossain, "Solar System Components," in *Photovoltaic Systems*, Cham: Springer International Publishing, 2022, pp. 95–192. doi: 10.1007/978-3-030-89780-2_5.